Industrial Crops & Products 188 (2022) 115579

Contents lists available at ScienceDirect

Industrial Crops & Products

journal homepage: www.elsevier.com/locate/indcrop

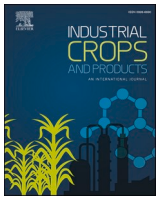

Production of lignin/cellulose acetate fiber-bead structures by electrospinning and exploration of their potential as green structuring agents for vegetable lubricating oils

J.F. Rubio-Valle, M.C. Sánchez, C. Valencia, J.E. Martín-Alfonso, J.M. Franco *

Pro2TecS – Chemical Process and Product Technology Research Center, Department of Chemical Engineering and Materials Science, ETSI, Universidad de Huelva, Campus de "El Carmen", 21071 Huelva, Spain

ARTICLE INFO

Keywords:
Electrospun nanofibers
Lignocellulose
Lubricant
Oleogel
Rheology

ABSTRACT

In this work we developed electrospun lignin/cellulose acetate fiber-bead nanostructures and explored their potential as structuring agents for vegetable oils to be used as eco-friendly lubricating oleogels. A variety of nanostructures were obtained from solutions containing 20 or 30 wt. % eucalyptus Kraft lignin (EKL) and cellulose acetate (CA) in variable weight ratios from 100:0 to 60:40 in an *N*,*N*-dimethylformamide/acetone mixture. The EKL/CA solutions were characterized in physicochemical terms from viscosity, surface tension and electrical conductivity measurements. Also, the electrospun nanostructures were characterized morphologically by scanning electron microscopy. Their morphology was found to be strongly dependent on the rheological properties of the biopolymer solution. Electrospun EKL/CA beaded nanofibers and well-developed uniform nanofiber mats allowed oleogels to be easily obtained by simply dispersing them in castor oil whilst nanoparticle clusters gave rise to unstable dispersions. The rheological properties of these gel-like dispersions can be tailored through the membrane concentration and/or EKL/CA ratio and depend to a large extent on the morphology of the electrospun nanostructures. The rheological and tribological properties of the oleogels were comparable to those previously reported for conventional and other bio-based lubricating greases. Overall, electrospun EKL/CA nanofibers allow easy, efficient structuring of vegetable oils to obtain oleogels holding potential for use as lubricants.

1. Introduction

In recent decades, interest in replacing petroleum-based products with more eco-friendly alternatives has grown steadily. Crude oil is becoming an increasingly limited and expensive resource, and also a major contributor to environmental pollution, global warming and climate change. The need to preserve the environment, and the increasing scarcity of petroleum, have led some to explore sustainable solutions (Anand and Chhibber, 2006). The lubricant sector estimates that approximately 55 % of the amount of lubricants marketed each year ends up in the environment (Syahir et al., 2017). Most commercially available lubricating greases are complex formulations consisting mainly of mineral or synthetic oils and thickeners that are neither biodegradable nor renewable (National Lubricating Grease Institute, 2006; Panchal et al., 2017). The rheological properties of lubricating greases, which determine the NLGI grade traditionally used to classify them (National Lubricating Grease Institute, 2006), and other functional properties of these products, are mainly a result of the structure formed by the thickener, usually composed of entangled fibers, polymeric chains or other types of structural units (National Lubricating Grease Institute, 2006). One possible solution to alleviate these environmental problems other than replacing mineral and synthetic oils with natural (vegetable) oils is using natural fibers and biopolymers to thicken and/or structure oils (Gallego et al., 2015a; Sánchez et al., 2011). Extensive research has so far been conducted to identify effective, sustainable structuring or thickening agents for oily media including natural polymers such as chitosan and chitin (Sánchez et al., 2011), cellulose derivatives (Gallego et al., 2015b) and more complex lignocellulosic materials (Cortés-Triviño et al., 2018; Gallego et al., 2015a; Núñez et al., 2011) such as lignin fractions (Borrero-López et al., 2018a, 2018b; Cortés-Triviño et al., 2017; Zeng et al., 2003). However, making these biopolymers compatible with oils usually requires some chemical

* Corresponding author.
E-mail address: franco@diq.uhu.es (J.M. Franco).

https://doi.org/10.1016/j.indcrop.2022.115579
Received 18 May 2022; Received in revised form 27 August 2022; Accepted 30 August 2022

modification such as epoxidation (Cortés-Triviño et al., 2018), methylation (Martín Alfonso et al., 2009; Núñez et al., 2012), ethylation (Martín-Alfonso et al., 2011), acylation (Sánchez et al., 2011), or polyurethane formation (Borrero-López et al., 2020b; Gallego et al., 2015a). Even though the final formulations can be deemed biobased, inert and nontoxic, many of the production procedures involve relatively complex chemical reactions, and using hazardous chemicals and solvents. Therefore, alternative, cleaner processes and methodologies should be found. One potential way of overcoming the previous shortcomings is to obtain nanostructures by electrospinning. The high porosity, nanometric size and high surface/volume ratio of electrospun nanostructures may allow a three-dimensional percolation network to be formed by effect of enhanced physical interactions with the lubricating oil (Borrego et al., 2021; Rubio-Valle et al., 2021a, 2021b).

As a possible raw material, lignocellulosic biomass containing various natural polymers is one renewable material increasingly used to formulate end-use products and develop innovative applications such as the implementation of nanofibers (Adam et al., 2020). Unlike other sources such as sugary or starchy biomass, lignocellulosic biomass is inexpensive, abundant, widely distributed and not intended for food consumption (Prasad et al., 2016). Also, it can be obtained from a variety of forest species. One of the most abundant, renewable and affordable types of lignocellulosic residues comes from the pruning of eucalyptus trees. Lignocellulosic biomass consists mainly of cellulose (35–83 %), hemicellulose (0–30 %), lignin (1–43 %) and various minor compounds such as tannins and waxes (Bajpai, 2016; Kobayashi and Fukuoka, 2013). The potential of lignocellulosic biomass lies largely in its high content in carbohydrates (particularly cellulose and hemicelluloses) (Mascal and Nikitin, 2010). By contrast, lignin has been much less widely used to date despite its being a renewable resource with the potential for industrial use (Gellerstedt and Henriksson, 2008; Laurichesse and Avérous, 2014). Although lignin production is estimated at 40–50 Mt/yr, it is scarcely used to obtain high added-value products (Pelaez-Samaniego et al., 2016; Xi et al., 2018) as the result of its complex chemical structure — so much so that most often lignin is managed as a residue and burned to obtain energy. However, lignin offers several benefits to be used in formulated products. Bearing in mind a possible application as structuring or thickening agent for lubricating oils, lignin streams obtained from pulping processes, such as the Kraft lignin, are rather recalcitrant towards degradation reactions, showing high stability against temperature and oxidation. For instance, onset temperatures for thermal degradation in the range 140–200ºC have been reported for Kraft lignins under inert atmosphere (Borrero-López et al., 2020a), whereas oxidation only occurs under sever conditions (presence of oxidizing agents such as nitrobenzene, metal oxides or oxygen, and catalysts, alkaline medium and rather high temperatures) (Vangeel et al., 2018; Costa el al, 2021). On the contrary, lignin has been shown to have antioxidant properties (Kasprzycka-Guttman and Odzeniak, 1994; Kaur and Uppal, 2015) and particularly a high antioxidant capacity in vegetable oils (Jedrzejczyk et al., 2021). Besides, the biodegradability and low ecotoxicity of lignin and some derived polymers and oleogels have also been previously demonstrated (Tuomela et al., 2020; Polman et al., 2020; Fajardo et al., 2021).

Electrospun lignin nanofibers have scarcely been developed for a number of reasons including the heterogeneous chemical composition of lignin, its highly branched structure and the presence of low molecular weight compounds forming by degradation during the biomass delignification process. As a result, electrosprayed particles and nonuniform structures consisting of particles or globules distributed along filaments (Aslanzadeh et al., 2016; Dallmeyer et al., 2010) in so-called "BOAS" (beads on-a-string) (Oliveira et al., 2006) are frequently obtained as a consequence of lignin chains not entangling to an adequate extent in solution (Dallmeyer et al., 2010). Therefore, lignin electrospinning procedures typically involve blending it with a second (dopant) polymer to obtain more uniform nanofibers and improve processability as a result (Aslanzadeh et al., 2016; Baker and Rials, 2013; Dallmeyer et al., 2014b; Stojanovska et al., 2019). By virtue of its high electrospinnability (Konwarh et al., 2013; Liu and Hsieh, 2002), and the ability to modulate its affinity for an oily medium through the degree of acetylation, cellulose acetate is a suitable doping polymer or biopolymeric component for developing lignin-based nanostructures; also, it is a biodegradable, renewable, biocompatible material that can be easily obtained from cellulose (Bifari et al., 2016).

In this work, lignin and cellulose acetate-based electrospun nanosized fiber-bead structures were assessed as structuring agents for vegetable lubricating oils with a view to developing a new way to valorize lignin residues with ecological, economic and social advantages. For this purpose, different types of nanostructures were developed by using variable proportions of eucalyptus kraft lignin (EKL) and cellulose acetate (CA). The rheological and tribological properties of the resulting oleogels were related to the morphological properties of the electrospun membranes.

Table 1
Nomenclature for electrospun nanostructures of variable EKL:CA weight ratios.

Sample code	EKL (wt. %)	CA (wt. %)
EKL100-CA0	100	0
EKL90-CA10	90	10
EKL80-CA20	80	20
EKL70-CA30	70	30
EKL60-CA40	60	40

2. Material and methods

2.1. Materials

Eucalyptus kraft lignin (EKL) was kindly supplied by INIA-CSIC (Madrid, Spain). The material was previously characterized elsewhere (Borrero-López et al., 2020a). Cellulose acetate (CA; M_n = 30,000 g/mol), *N*,*N*-dimethylformamide (DMF) and acetone (Ac) were purchased from Merck Sigma–Aldrich (Darmstadt, Germany). Castor oil (Guinama, Valencia, Spain) was used as base oil to prepare the oleogels. The fatty acid composition and main physical properties of this vegetable oil can be found elsewhere (Quinchia et al., 2010).

2.2. Production of EKL/CA nanostructures

2.2.1. Preparation of EKL/CA solutions

EKL and CA were dissolved in a 1:2 v/v DMF/Ac mixture, at 20 and 30 wt. % total concentrations, in different weight ratios (see Table 1). All solutions were prepared by magnetic stirring at 500 rpm at room temperature for 24 h.

2.2.2. Electrospinning

EKL/CA solutions were electrospun in a chamber from DOXA Microfluidics (Málaga, Spain). A volume of 10 mL was placed in a syringe fitted with a 21-G needle that was attached to the holder in a horizontal configuration and coupled to a high-voltage power supply providing 17 kV. The needle tip was placed 15 cm from an aluminum collector plate and a positively charged jet from the syringe tip was projected onto the negatively charged collector. Nanostructures were then carefully removed from the collector plate. All experiments were performed at room temperature (22 ± 1 °C) and almost constant relative humidity (45 ± 1 %).

2.3. Preparation of oleogels

Selected electrospun nanostructures were dispersed at 5, 10, and 15 wt. % concentrations in castor oil at room temperature under gentle agitation, using a RW 20 IKA stirrer (75 rpm) coupled to an anchor impeller (Borrero-López et al., 2020b). The resulting gel-like dispersions

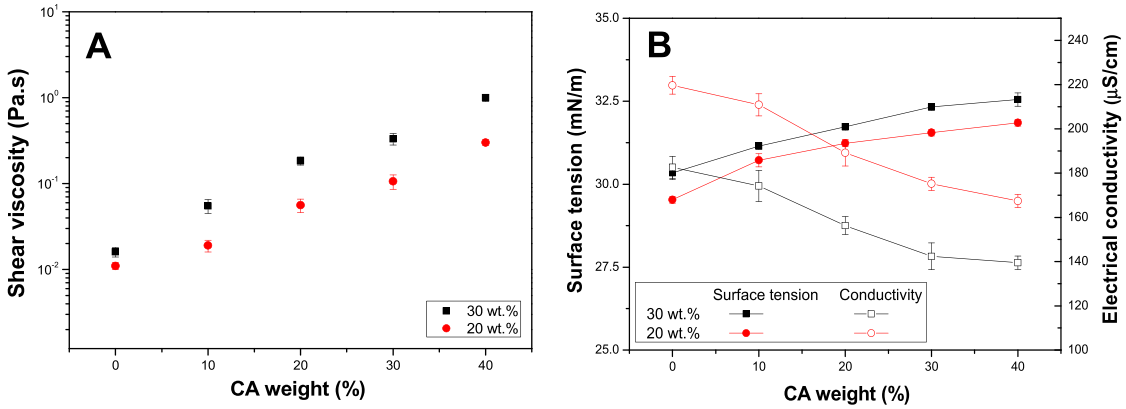

Fig. 1. Influence of the EKL:CA ratio and total polymer concentration on A) the dynamic viscosity, and B) surface tension and electrical conductivity of the solutions.

were stored at room temperature for further characterization.

2.4. Characterization techniques

2.4.1. EKL/CA solutions

The dynamic viscosity of the EKL/CA solutions was determined in an ARES (Rheometric Scientific, UK) controlled-strain rheometer at shear rates over the range 1–300 s^{-1}, using a Couette geometry (16 mm inner diameter and 1 mm gap width) at 25 °C. Surface tension measurements were made with a Sigma 703D force tensiometer from Biolin Scientific (Beijing, China). The surface tension of each solution was measured with a 39.2 mm wide × 0.1 mm thick platinum Wilhelmy plate at 25 °C. Electrical conductivity was measured with a CE GLP31 conductivity meter from Crison (Barcelona, Spain), the conductivity cell being previously calibrated with standard KCl solutions of known conductivity. All measurements were made at least three times.

2.4.2. Electrospun nanostructures

Electrospun nanostructures were characterized morphologically by scanning electron microscopy (SEM) in a JXA-8200 SuperProbe instrument from JEOL (Tokyo, Japan), using a secondary electron detector at an acceleration voltage of 15 kV. Nanostructures were previously sputtered with gold (Erdem et al., 2016). SEM images were analyzed with the open-source software FIJI ImageJ. From this image analysis, histograms of the particle and fiber size distributions, as well as overall porosity, were estimated by relating image pixels to length dimensions, i,e, determining the number of pixels contained in one micrometre (Hotaling et al., 2015). The average particle and fiber diameters were then calculated from these size distributions as arithmetic means. Each observation was the result of 100 random measurements at the same magnification.

Thermal stability of electrospun nanostructures was evaluated by measuring mass losses versus temperature in a thermogravimetric analyzer, model Q-50 (TA Instrument Waters, USA) under N_2 purge. 5-10 mg of sample were placed on a platinum pan and heated from 50° to 600°C at 10 °C/min.

2.4.3. EKL/CA nanofiber-structured oleogels

Oleogels were characterized in rheological terms with a controlled-stress Rheoscope rheometer from Thermo Scientific (Waltham, MA, USA), using a serrated plate-plate geometry (20 mm diameter and 1 mm gap). Small-amplitude oscillatory shear (SAOS) tests were conducted within the linear viscoelastic region (frequency range 0.03–100 rad/s) at 25 °C. Stress sweep tests were previously performed to identify the prevailing linear viscoelastic regime. Viscous flow measurements were made with the same rheometer at shear rates from 10^{-2} to 10^{2} s^{-1}, using a serrated plate-plate geometry (25 mm diameter and 1 mm gap).

Tribological measurements were made in a Physica MCR-501 rheometer from Anton Paar (Graz, Austria) equipped with a tribological cell. The cell consisted of a 6.35 mm diameter steel ball rotating on three 45° inclined rectangular steel plates onto which the oleogel samples acting as lubricants were spread. A constant normal load of 20 N and a rotational speed of 10 rpm were used for 10 min. Effective normal forces and friction coefficients were calculated from the applied axial force and torque measured by the rheometer as described elsewhere for this geometry (Heyer and Läuger, 2009).

Oleogel microstructure was examined with an AURIGA scanning electron microscope from Zeiss (White Plains, NY, USA) coupled to a secondary electron detector operating at an acceleration voltage of 20 kV. Oleogels were treated with a chemical fixing agent (Malm et al., 2009) and subsequently sputtered with gold to a very thin layer in order to improve the accuracy of the observations (Stokroos et al., 1998).

2.5. Statistical analysis

The data of measured properties and selected parameters were subjected to analysis of variance (ANOVA) and significant differences between means identified with a comparison test at $p < 0.05$.

3. Results

3.1. Physicochemical properties of the EKL/CA solutions

The electrospinning performance of a large variety of biopolymer solutions and the use of the resulting nanofibers have been widely reported and reviewed (Kakoria and Sinha-Ray, 2018; Madruga and Kipper, 2021; Wilk and Benko, 2021). Electrospinnability is known to depend on the surface tension, viscosity and electrical conductivity of the solution, which in turn are a function of the nature of the biopolymer and its concentration (Borrego et al., 2021; Rubio-Valle et al., 2021a, 2021b).

Fig. 1A shows the dynamic viscosity for the EKL/CA solutions. All exhibited Newtonian behavior throughout the shear rate range studied. As can be seen, dynamic viscosity increased with the total EKL/CA concentration and decreased with increasing EKL:CA weight ratio. As expected, the higher the proportion of CA, the higher was the viscosity (Jia et al., 2018). Fig. 1B shows the surface tension and electrical conductivity of the solutions as a function of the CA weight proportion and total biopolymer concentration. As can be seen, surface tension slightly increased with increasing amount of CA (i.e., with decreasing EKL:CA ratio) and total biopolymer concentration. The differences were statistically significant, the surface tension ranging from 29.53 mN/m for the CA-free system (EKL100–0CA) at 20 wt. % to 32.55 mN/m for the EKL60-CA40 system at 30 wt. %. The electrical conductivity varied more markedly with the total biopolymer concentration and EKL:CA weight ratio. Thus, as expected from the lower molecular weight and greater

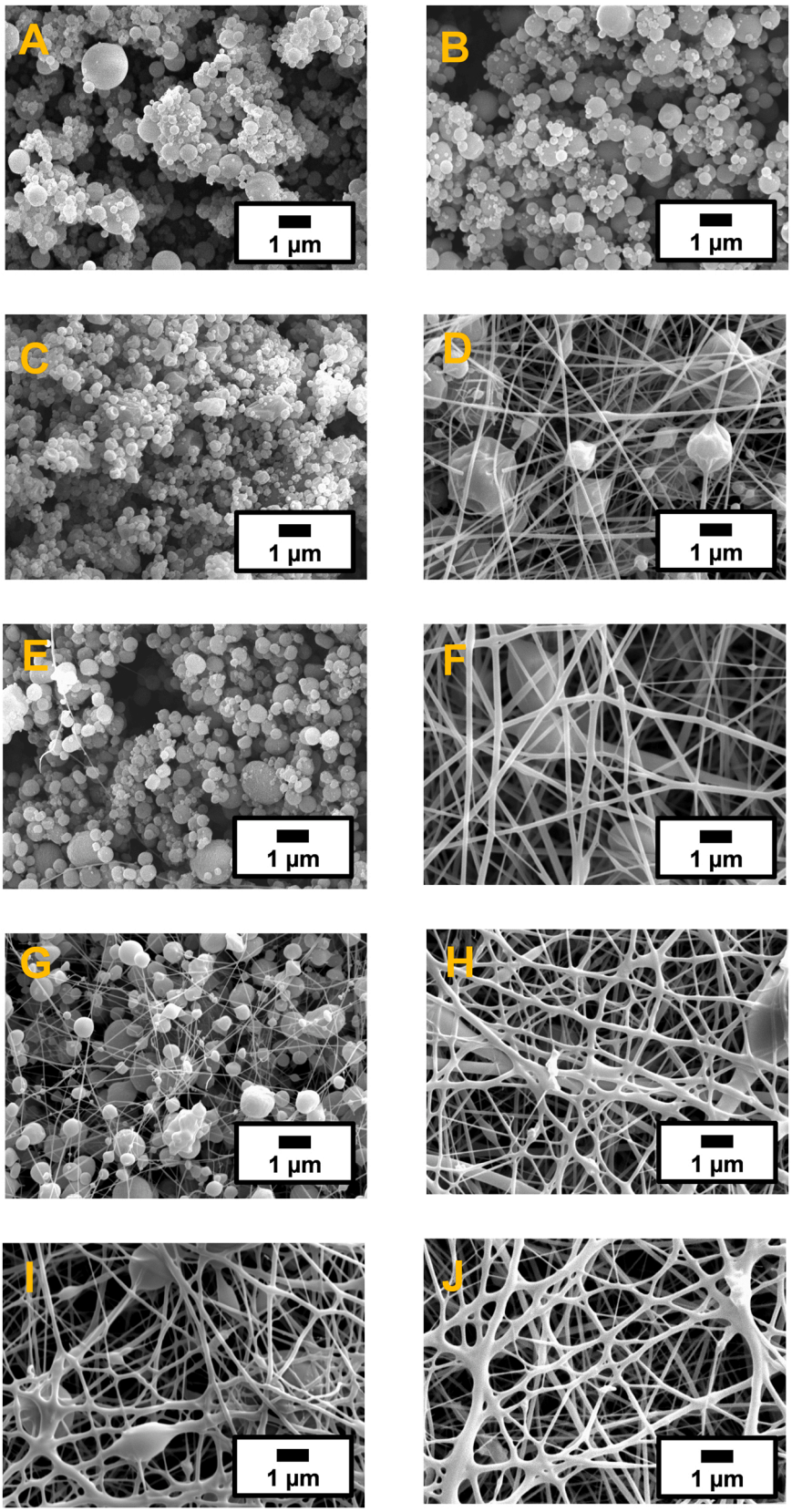

Fig. 2. SEM images of electrospun nanostructures obtained from solutions with a 20 or 30 wt. %. total biopolymer concentration and variable EKL:CA weight ratios. A) EKL100 at 20 wt. %., B) EKL100 at 30 wt. %., C) EKL90-CA10 at 20 wt. %., D) EKL90-CA10 at 30 wt. %., E) EKL80-CA10 at 20 wt. %., F) EKL80-CA10 at 30 wt. %., G) EKL70-CA30 at 20 wt. %., H) EKL70-CA30 at 30 wt. %., I) EKL60-CA40 at 20 wt. %. and J) EKL60-CA40 at 30 wt. %.

Table 2
Average particle and fiber diameters, and overall porosity, of the EKL/CA electrospun nanostructures.

Solution concentration (wt. %)	EKL:CA ratio	Average particle diameter (μm)	Average fiber diameter (μm)	Porosity (%)
20	100:0	0.91^{A}	–	36.4^{α}
	90:10	0.59^{B}	–	37.2^{β}
	80:20	0.47^{C}	0.07^{a}	37.7^{β}
	70:20	0.42^{C}	0.21^{b}	43.1^{γ}
	60:40	–	0.53^{c}	46.8^{δ}
30	100:0	0.69^{D}	–	38.9^{ε}
	90:10	0.61^{E}	0.26^{b}	45.2^{ϕ}
	80:20	0.51^{C}	0.48^{c}	$46,1^{\delta}$
	70:30	–	0.61^{d}	48.3^{φ}
	60:40	–	0.72^{e}	50.8^{χ}

Note: Values with different superscripts along the same column were significantly different at $p < 0.05$.

polarity of EKL —a chemical structure consisting of phenolic, and aliphatic hydroxyl and carboxyl moieties—, electrical conductivity decreased with increasing proportion of CA. Electrical conductivity also decreased with increasing concentration of biopolymer from 20 to 30 wt. %. The decrease can be ascribed to a reduced mobility of entangled macromolecules at high biopolymer concentrations, specifically above the overlap concentration (Rubio-Valle et al., 2021a, 2021b).

3.2. Characterization of electrospun nanostructures

Fig. 2 shows SEM images for electrospun nanostructures obtained from solutions containing 20 or 30 wt. % concentration of biopolymer in variable EKL:CA weight ratios. As can be seen, electrospinning failed to produce lignin nanofibers unless a certain amount of CA was added — in its absence, it gave electrosprayed, largely submicrometric particles (Fig. 2A and B). A similar result was obtained when a small amount of CA (10 or 20 wt. %) was added to the lignin solutions at a 20 wt. % total biopolymer concentration (see Fig. 2C and E). However, an 80:20 EKL:CA weight ratio led to the formation of isolated filaments interconnecting particles (Fig. 2E), and especially with a 70:30 EKL:CA weight ratio (Fig. 2G). Even lower EKL:CA ratios produced the typical BOAS (beads-on-a-string) structure (Fig. 2I). Increasing the total biopolymer concentration to 30 wt. % caused these nanostructures to appear at higher EKL:CA weight ratios, and the amount and density of nanofibers to increase. Thus, interconnected fibers with embedded particles were observed above a 90:10 EKL:CA weight ratio (Fig. 2D), whereas uniform mats entirely consisting of fibers were clearly detected at CA proportions above 20 wt. % (Fig. 2H and J).

These results are consistent with those of other authors (Borrego et al., 2021; Dallmeyer et al., 2014a, 2010), who found the addition of a certain amount of dopant polymer to be essential for bead-free and/or uniform lignin nanofibers to form by electrospinning. As well known, high-molecular-weight and linear polymers, like CA, are more easily electrospinnable than low-molecular-weight, branched and heterogenous polymers, like lignin, not entangling to an adequate extent in solution. Accordingly, CA-free lignin solutions are not really electrospinnable, whereas increasing the CA proportion helps to produce and stabilize the jet formation, thus reducing the number of isolated or embedded submicrometric particles. In addition, the morphology of nanostructures containing high CA proportions was consistent with that reported for pure CA electrospun nanofiber mats as regards architectural properties such as fiber size, overall porosity, and pore size and geometry (Konwarh et al., 2013; Lee et al., 2018; Nguyen et al., 2013). These results underline the importance of cellulose acetate in lignin-based mats.

On the other hand, it is well known that proper electrospinnability of polymer solutions can be achieved with a suitable combination of electrical conductivity, surface tension and rheological characteristics. Both an increase in conductivity and a decrease in surface tension favour jet formation and the stretching of nanofibers, whereas a high viscosity retards the stretching, but reduces and/or prevents the filament breakage, thus increasing fiber diameter. In general, the higher the CA content or the total polymer concentration, the higher the solution viscosity, favouring nanofiber formation and increasing fiber diameter. On

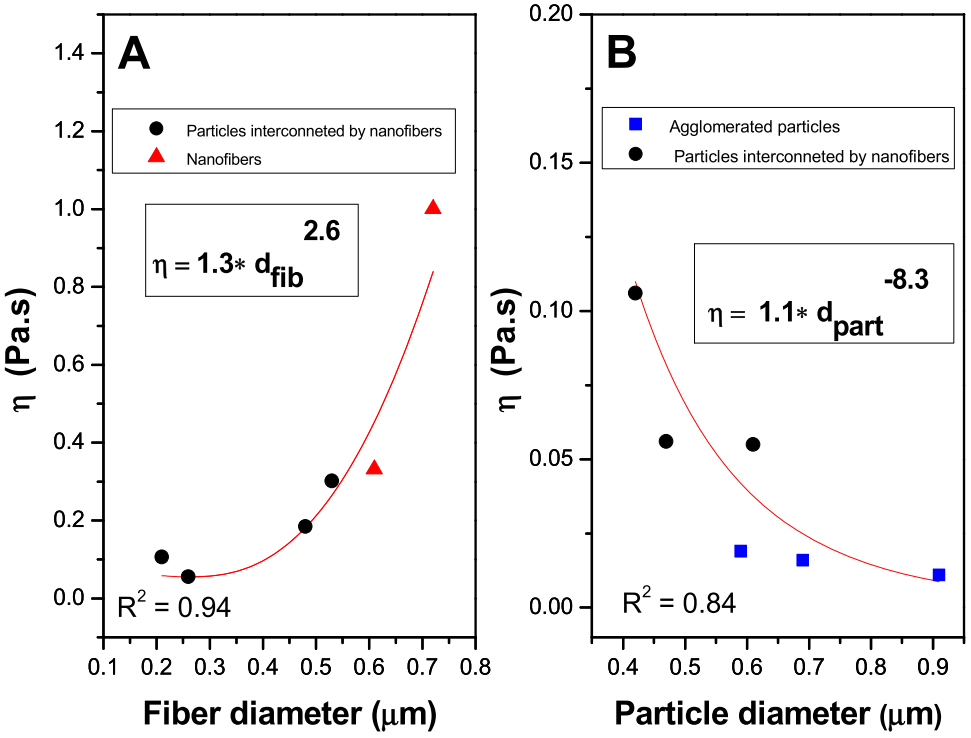

Fig. 3. Relationships between the viscosity of the electrospun solutions and A) the average fiber diameter, and B) average particle diameter of the resulting nanostructures.

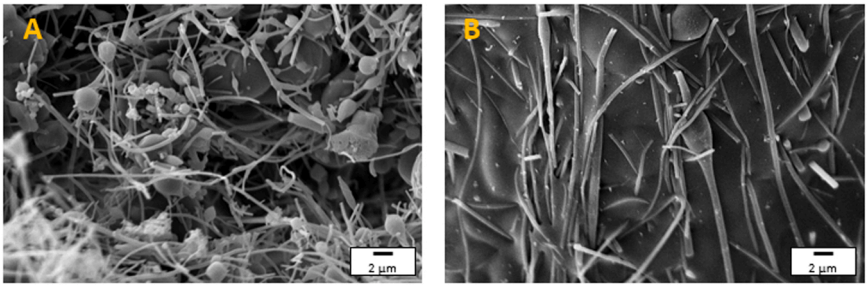

Fig. 4. SEM images of the nanostructures of selected oleogels prepared with A) EKL90-CA10 (30), and B) EKL70-CA30 (30), both at 15 wt. %.

the contrary, the higher the lignin proportion, the higher the electrical conductivity and the lower the surface tension, thus promoting filament thinning and/or disruption, and essentially giving rise to electrosprayed particles. Table 2 shows the average diameters of particles and fibers calculated from the image analysis of SEM micrographs, as well as the overall porosity of the electrospun nanostructures. As can be seen, fiber average diameter invariably increased with increasing CA content and total biopolymer concentration in solution, from very thin filaments of 0.07 µm with EKL80-CA20, which was prepared from a 20 wt. % solution, to thick fibers of average size 0.72 µm with the EKL60-CA40 nanostructure, which was obtained from a 30 wt. % solution. On the other hand, the average diameter of particles decreased with increasing CA content and total biopolymer concentration. Also, porosity increased with increasing concentration of polymers and CA content by effect of the reduced number of particles and/or beads in the filaments (BOAS).

Fig. 3 illustrates the relationships between the viscosity of the electrospun solutions and the average size of the particles and fibers obtained. As can be seen, a relationship between solution dynamic viscosity and mean fiber diameter clearly existed in the form of an empirical power-law:

$$\eta = a \bullet d_{fib}^{b} \quad (1)$$

where η is the dynamic viscosity, d_{fib}, the mean fiber size, and a and b are adjustable parameters. In the experimental range studied, b was 2.6. On the other hand, an inverse relationship existed in particle-based nanostructures:

$$\eta = a \bullet d_{part}^{-b} \quad (2)$$

with a negative exponent (8.3). Therefore, the prevailing architecture (viz., agglomerated particles, particles interconnected by filaments or uniform nanofibers) can be predicted from the solution viscosity, and so can the resulting fiber and/or particle mean size in electrospun membranes. The average nanofiber diameter decreased almost linearly with decreasing surface tension and increasing electrical conductivity. Therefore, the resulting fiber-bead nanostructures could be tailored to some extent by adjusting the solution properties under identical electrospinning conditions.

The thermal stability of these lignin-based electrospun fiber-bead structures has also been explored by means of thermogravimetric analysis (TGA). Fig. S1 in the Supporting Information shows TGA curves in the form of the derivative function of weight loss versus temperature for selected samples. As expected, the thermal degradation profile of the electrospun nanostructure comprising only Kraft lignin (EKL100-CA0) is very similar to those previously reported for Eucalyptus Kraft lignins (Borrero-López et al., 2018a, 2018b, 2020a). As well-known, lignin thermal degradation occurs over an extended temperature range of 130–500 °C, which can be divided in several stages. Initially, hydroxyl groups dehydration starts to occur at around 150ºC, followed by the cleavage of aryl alkyl-ether linkages between 150 and 300 °C and the splitting of aliphatic side chains from the aromatic rings, starting at around 290 °C. Finally, carbon-carbon cleavage between lignin

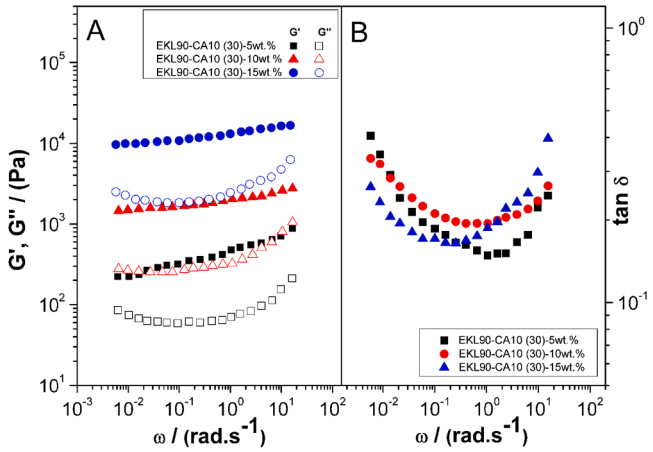

Fig. 5. Frequency-dependence of A) the storage (G') and loss (G'') moduli and B) the loss tangent, for oleogels prepared with the EKL90-CA10(30) nanostructure at 5, 10 and 15 wt. %.

structural units occurs in the temperature range of 350–450 °C (Laurichesse and Avérous, 2014; Borrero-López et al., 2018a, 2018b). The temperatures associated to the maximum degradation rate in each stage are shown in Table S1 (see Supporting Information), the main degradation event being found at around 325 ºC. The thermal degradation profiles of the different nanostructures are only marginally modified when CA is included. The main differences are that the main degradation peak became more important and the shoulder appearing at around 290 ºC was also more apparent, which is due to the degradation pattern of CA, also included in Fig. S1 for the sake of comparison.

3.3. Oil-structuring ability of EKL/CA nanofiber mats

Only those EKL:CA nanostructures consisting of BOAS or well-developed uniform nanofiber mats formed physically stable gel-like dispersions in castor oil. On the other hand, those consisting of electrosprayed particles only gave unstable dispersions from which the oil eventually separated. This was a result of the oleogels forming largely through physical interactions between the oil and the three-dimensional nanofiber network, where the oil was adsorbed by entrapment in voids. Those physical interactions were mainly of the intermolecular hydrophobic and van der Waals types (Ding et al., 2006; Zhang et al., 2020). Therefore, obtaining nanosized fibers by electrospinning is essential for a stable nanodispersion to form by effect of the large specific surface area and high surface/volume ratio —a trait shared with lignin/PVP composites (Borrego et al., 2021). Electrospun nanostructures roughly retained their morphology in the oleogels upon dispersion of nanofiber mats. As can be seen in Fig. 4, the oleogels prepared with EKL90-CA10 (30) and EKL70-CA30(30) nanostructures at 15 wt. % comprised BOAS in the former case and exhibited a more uniform network consisting predominantly of fibers in the latter. Consequently, oleogel

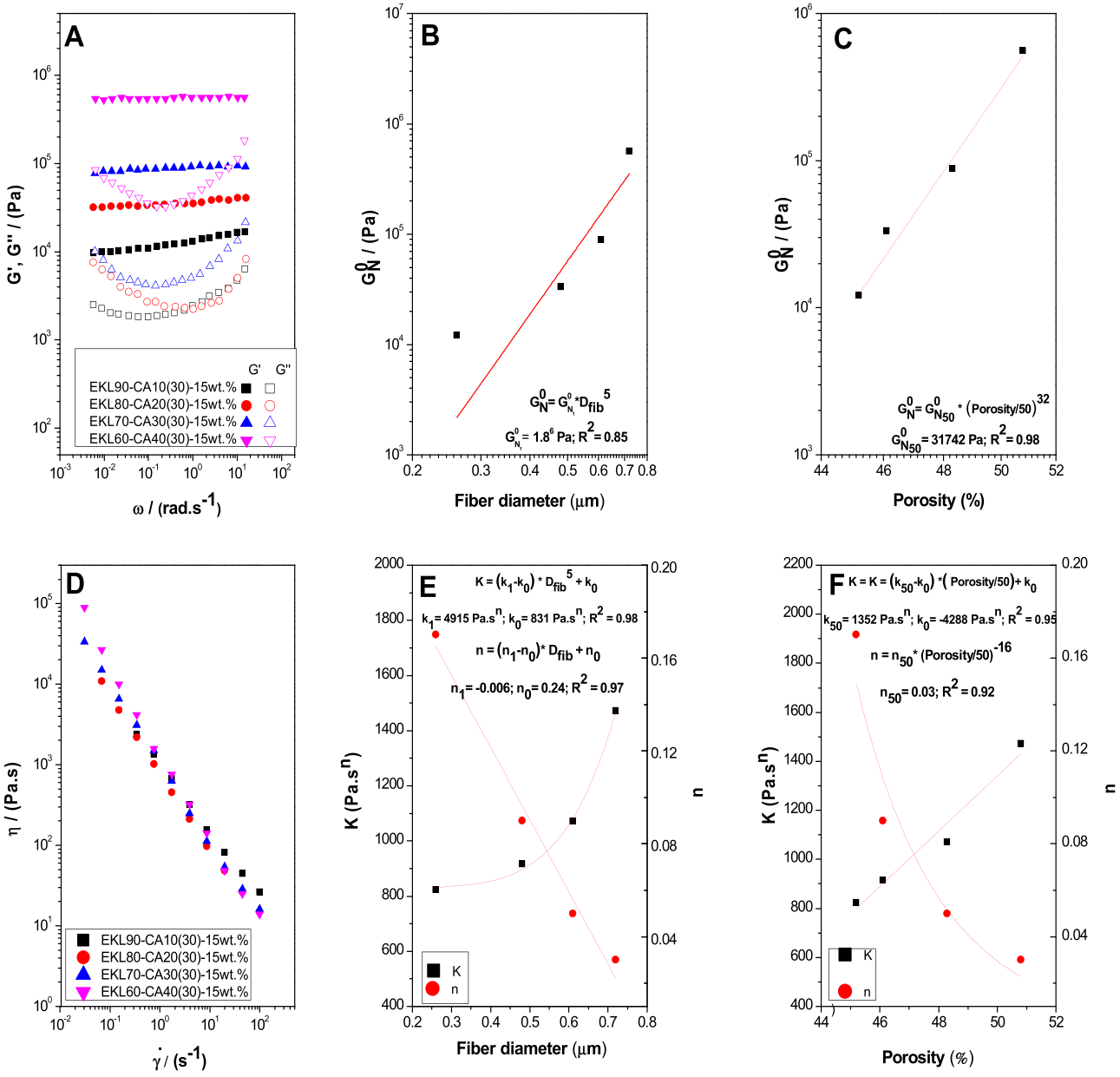

Fig. 6. Influence of the EKL:CA weight ratio and associated nanostructure morphological characteristics on the rheological properties of the oleogels: A) variation of G' and G'' with frequency; dependence of the plateau modulus with B) the average fiber diameter and C) nanostructure porosity; D) evolution of viscosity with shear rate, and dependence of the consistency and flow indexes with E) the average fiber diameter and F) nanostructure porosity. Note: fitting parameters with subscripts 0, 1 or 50 provided in the insets correspond to values associated to fiber diameters of 0 and 1 μm or 0 % and 50 % porosity, not necessarily with physical meaning and only valid to describe the evolutions of the rheological parameters in the experimental ranges of fiber diameter and porosity.

microstructure was essentially dictated by the morphology of the electrospun nanostructures used for structuring —which, as shown below, determine the rheological properties of the oleogels to a large extent.

The nanostructure obtained from the 30 wt. % EKL/CA solution with a 90:10 EKL:CA ratio, sample EKL90-CA10(30), was dispersed at a concentration of 5, 10 and 15 wt. % in castor oil at room temperature. Fig. 5A shows the mechanical spectra for the resulting oleogels as a function of the concentration of the electrospun nanostructure. The frequency-dependence of the SAOS functions (viz., G' and, G'', which are the storage and loss moduli, respectively) was typical of gel-like dispersions and qualitatively similar at the three nanofiber concentrations, G' exceeding G'' throughout the frequency range. Besides, both SAOS functions considerably increased —by almost two decades— with increasing concentration of the electrospun nanostructure. By contrast, as can be seen from the loss tangent ($\tan\delta = G''/G'$) versus frequency plots of Fig. 5B, the relative elasticity was almost unaffected.

These mechanical spectra very much resemble those reported for conventional lubricating greases (Delgado et al., 2006a; Martín-Alfonso et al., 2007; Sánchez et al., 2014). Although, the SAOS functions for lubricating greases essentially depend on consistency —which is dictated by thickener content—, the mechanical spectrum for the oleogel containing the EKL90-CA10 (30) nanostructure at 15 wt. % matched fairly well those for the most commonly used NLGI grade 2 lubricating greases. Therefore, we chose to use that concentration to assess the effect of the EKL:CA weight ratio on the rheological properties of the oleogels. Fig. 6A shows the variation of the SAOS functions for lubricating oleogels prepared with nanostructures in variable EKL:CA weight ratios. Again, the rheological response was qualitatively similar throughout the frequency range, but G' and G'' increased markedly with decreasing EKL:CA weight ratio by effect of *i)* an increased proportion of

Table 3
Rheological and tribological parameters for EKL:CA nanofiber-structured oleogels.

Oleogel	K (Pa.s^n)	n	Friction coefficient	Wear scar diameter (μm)
EKL90-CA10 (30)-15 wt. %	813.1^{a}	0.17^{A}	0.067$^{\alpha}$	191^{Aa}
EKL80-CA20 (30)-15 wt. %	915.2^{b}	0.09^{B}	0.105$^{\beta}$	313^{Bb}
EKL70-CA30 (30)-15 wt. %	1070.1^{c}	0.05^{C}	0.110$^{\beta}$	349^{Cc}
EKL60-CA40(30)-15 wt. %	1471.5^{d}	0.03^{D}	0.121$^{\gamma}$	356^{Cc}

Note: Values with different superscripts along the same column were significantly different at $p < 0.05$.

the component with the higher average molecular weight (CA) in the nanostructure and *ii*) its beneficial effect on morphological properties (viz., thicker, more uniform nanofibers and higher porosity). Aiming to illustrate the effect of the morphology of electrospun nanostructures on the viscoelastic response of the oleogels, the plateau modulus (G_N^0), as defined elsewhere (Ferry, 1980), is plotted in Fig. 6B and C as a function of average fiber size and porosity, showing a power-law evolution with both parameters.

On the other hand, Fig. 6D shows the viscous flow curves for EK:CA nanofiber-structured oleogels as a function of EKL:CA weight ratio. The power-law model adequately fits the observed shear thinning behavior:

$$\eta = K \bullet \dot{\gamma}^{\,n-1} \tag{3}$$

where K and n are the consistency index and the flow index, respectively. Table 3 shows the values of both fitting parameters for the different oleogels. Although the influence of EKL:CA weight ratio on viscosity is smaller, K and n were also found to depend on the morphological properties of the electrospun nanostructures, which in turn depended on the EKL:CA ratio. Fig. 6E and F illustrate the trends followed by K and n as a function of the average fiber diameter and nanostructure porosity. It is interesting to note that K varies potentially and linearly with fiber diameter and porosity, respectively, whilst conversely n depends linearly and potentially with them in the experimental ranges achieved for these morphological parameters. In general, K increased with increasing proportion of CA, whereas the flow index decreased and was extremely low in all cases —which is typical of materials with markedly non-Newtonian properties such as conventional lubricating greases (Delgado et al., 2006b). Overall, these results confirm that the rheological properties of the resulting oleogels depend to a large extent on the morphological properties of the nanostructures obtained during the electrospinning process.

3.4. Lubricating performance of structured oleogels based on EKL/CA nanofiber mats

Table 3 collects the friction coefficients obtained in a ball-on-three plate steel–steel tribological configuration and the average diameter of the resulting wear scars generated on the plates. Most of the samples exhibited adequate friction coefficients in addition to wear diameters comparable to those for conventional greases (Gallego et al., 2016; Sánchez et al., 2014), or chemically functionalized cellulose or lignin-based oleogels (Cortés-Triviño et al., 2019; Delgado et al., 2020; Gallego et al., 2016) used as lubricants under similar conditions. However, the oleogel prepared with the EKL90-CA10(30) nanostructure exhibited an exceptionally low friction coefficient and a reduced wear scar size. Possibly, this presumably weaker BOAS nanostructure consisting of particles of much thinner fibers (Fig. 2D) allowed oil to be more easily released into the contact area, thus facilitating the formation of a fluid film, and decreasing wear and friction in the mixed lubrication regime as a result —in contrast to the more extensive and robust three-dimensional nanofiber networks observed at higher CA proportions, which must have retained the oil more efficiently. Moreover, a softer rheological response of this oleogel may have facilitated penetration of the thickener (i.e., the EKL/CA nanostructure) into the tribological contact zone.

4. Conclusions

Various types of nanostructures were obtained by electrospinning solutions of eucalyptus Kraft lignin (EKL) and cellulose acetate (CA) in a 1:2 v/v mixture of DMF and acetone. The surface tension and electrical conductivity of the EKL/CA solutions enabled their electrospinning. However, the morphology of the resulting nanostructures was strongly dependent on the dynamic viscosity of the solution, which in turn was dictated by the overall EKL/CA concentration and EKL:CA weight ratio. Solutions containing 20 wt. % concentration in high EKL weight ratios formed electrosprayed submicron particles or nanoparticles connected by thin filaments, whereas solutions of a 30 wt. % concentration and/or containing an increased proportion of CA formed beaded nanofibers (BOAS) and uniform fiber mats. Particle diameter and fiber width were related to the dynamic viscosity of EKL/CA solutions.

EKL/CA electrospun nanostructures consisting of filament-interconnected particles, BOAS or well-developed uniform nanofiber mats successfully structured castor oil and formed physically stable gel-like dispersions. The linear viscoelastic response of the oleogels was qualitatively similar but SAOS functions increased with nanostructure concentration and CA content. On the other hand, the relative elasticity of the oleogels was unaffected by the EKL/CA weight ratio. The morphological features of the electrospun nanostructures, i.e. the average fiber diameter and porosity largely influence the viscous and viscoelastic properties of the resulting oleogels. Overall, the EKL/CA electrospun fiber-bead structures gel-like dispersions in castor oil had adequate tribological properties on a par with those of conventional lubricating greases. However, the oleogel prepared with a nanostructure consisting of a relatively weak BOAS structure exhibited an exceptionally low friction coefficient and reduced wear as the likely result of the oil being more efficiently released into the lubricating contact zone.

Based on the experimental results, electrospinning of EKL/CA solutions can provide an efficient method for obtaining nanostructures capable of structuring vegetable oils to a different extent with a view to producing oleogels with rheological and tribological properties suitable for lubricating purposes. Also, using lignin as a thickener to obtain green lubricating greases can provide a new way of valorizing lignocellulosic waste with ecological, economic and social benefits.

CRediT authorship contribution statement

J.F. Rubio-Valle: conceptualization, investigation, methodology, formal analysis, data curation, writing-original draft, review & editing; **M.C. Sánchez:** methodology, formal analysis, data curation, supervision, review & editing; **C. Valencia:** conceptualization, methodology, validation, formal analysis, funding acquisition, project administration, supervision, review & editing; **J.E. Martín-Alfonso:** conceptualization, investigation, methodology, validation, supervision, formal analysis; **J. M. Franco:** conceptualization, investigation, methodology, validation, funding acquisition, project administration, supervision, writing-original draft, review & editing, All authors have read and agreed to the published version of the manuscript.

Declaration of Competing Interest

The authors declare that they have no known competing financial interests or personal relationships that could have appeared to influence the work reported in this paper.

Data availability

Data will be made available on request.

Acknowledgements

This work is part of Research Project RTI2018–096080-B-C21, funded by MCIN/AEI/10.13039/501100011033 and "ERDF A way of making Europe". J.F.R.-V. additionally acknowledges award of PhD Research Grant PRE2019–090632 from Spain's Ministry of Science and Innovation.

Appendix A. Supporting information

Supplementary data associated with this article can be found in the online version at doi:10.1016/j.indcrop.2022.115579.

References

Adam, A.A., Ojur Dennis, J., Al-Hadeethi, Y., Mkawi, E.M., Abubakar Abdulkadir, B., Usman, F., Mudassir Hassan, Y., Wadi, I.A., Sani, M., 2020. State of the art and new directions on electrospun lignin/cellulose nanofibers for supercapacitor application: a systematic literature review. Polymers (Basel) 12, 2884. https://doi.org/10.3390/polym12122884.

Anand, O.N., Chhibber, V.K., 2006. Vegetable oil derivatives: environment-friendly lubricants and fuels. J. Synth. Lubr. 23, 91–107. https://doi.org/10.1002/jsl.14.

Aslanzadeh, S., Zhu, Z., Luo, Q., Ahvazi, B., Boluk, Y., Ayranci, C., 2016. Electrospinning of colloidal lignin in Poly(ethylene oxide) N, N -dimethylformamide solutions. Macromol. Mater. Eng. 301, 401–413. https://doi.org/10.1002/mame.201500317.

Bajpai, P., 2016. Structure of lignocellulosic biomass 7–12. https://doi.org/10.1007/978-981-10-0687-6_2.

Baker, D.A., Rials, T.G., 2013. Recent advances in low-cost carbon fiber manufacture from lignin. J. Appl. Polym. Sci. 130, 713–728. https://doi.org/10.1002/app.39273.

Bifari, N., Bahadar Khan, E., A. Alamry, S., K, A, M.Asiri, Akhtar, K., 2016. Cellulose acetate based nanocomposites for biomedical applications: a review. Curr. Pharm. Des. 22, 3007–3019. https://doi.org/10.2174/1381612822666160316160016.

Borrego, M., Martín-Alfonso, J.E., Sánchez, M.C., Valencia, C., Franco, J.M., 2021. Electrospun lignin-PVP nanofibers and their ability for structuring oil. Int. J. Biol. Macromol. 180, 212–221. https://doi.org/10.1016/j.ijbiomac.2021.03.069.

Borrero-López, A.M., Santiago-Medina, J.F., Valencia, C., Eugenio, M.E., Martin-Sampedro, R., Franco, J.M., 2018. Valorization of Kraft lignin as thickener in castor oil for lubricant applications. J. Renew. Mater. 6, 347–361 https://doi:10.7569/JRM.2017.634160.

Borrero-López, A.M., Blánquez, A., Valencia, C., Hernández, M., Arias, M.E., Eugenio, M. E., Fillat, Ú., Franco, J.M., 2018. Valorization of soda lignin from wheat straw solid-state fermentation: production of oleogels. ACS Sustain. Chem. Eng. 6, 5198–5205. https://doi.org/10.1021/acssuschemeng.7b04846.

Borrero-López, A.M., Martín-Sampedro, R., Ibarra, D., Valencia, C., Eugenio, M.E., Franco, J.M., 2020a. Evaluation of lignin-enriched side-streams from different biomass conversion processes as thickeners in bio-lubricant formulations. Int. J. Biol. Macromol. 162, 1398–1413. https://doi.org/10.1016/j.ijbiomac.2020.07.292.

Borrero-López, A.M., Valencia, C., Franco, J.M., 2020b. Green and facile procedure for the preparation of liquid and gel-like polyurethanes based on castor oil and lignin: effect of processing conditions on the rheological properties. J. Clean. Prod. 277, 123367 https://doi.org/10.1016/j.jclepro.2020.123367.

Cortés-Triviño, E., Valencia, C., Franco, J.M., 2017. Influence of epoxidation conditions on the rheological properties of gel-like dispersions of epoxidized kraft lignin in castor oil. Holzforschung 71, 777–784. https://doi.org/10.1515/hf-2017-0012.

Cortés-Triviño, E., Valencia, C., Delgado, M.A., Franco, J.M., 2018. Rheology of epoxidized cellulose pulp gel-like dispersions in castor oil: Influence of epoxidation degree and the epoxide chemical structure. Carbohydr. Polym. 199, 563–571. https://doi.org/10.1016/j.carbpol.2018.07.058.

Cortés-Triviño, E., Valencia, C., Delgado, M.A., Franco, J.M., 2019. Thermo-rheological and tribological properties of novel bio-lubricating greases thickened with epoxidized lignocellulosic materials. J. Ind. Eng. Chem. 80, 626–632. https://doi.org/10.1016/j.jiec.2019.08.052.

Costa, C.A.E., Vega-Aguilar, C.A., Rodrigues, A.E., 2021. Added-value chemicals from lignin oxidation. Molecules 26, 4602. https://doi.org/10.3390/molecules26154602.

Dallmeyer, I., Ko, F., Kadla, J.F., 2010. Electrospinning of technical lignins for the production of fibrous networks. J. Wood Chem. Technol. 30, 315–329. https://doi.org/10.1080/02773813.2010.527782.

Dallmeyer, I., Ko, F., Kadla, J.F., 2014a. Correlation of elongational fluid properties to fiber diameter in electrospinning of softwood kraft lignin solutions. Ind. Eng. Chem. Res. 53, 2697–2705. https://doi.org/10.1021/ie403724y.

Dallmeyer, I., Lin, L.T., Li, Y., Ko, F., Kadla, J.F., 2014b. Preparation and characterization of interconnected, kraft lignin-based carbon fibrous materials by electrospinning. Macromol. Mater. Eng. 299, 540–551. https://doi.org/10.1002/mame.201300148.

Delgado, M.A., Valencia, C., Sánchez, M.C., Franco, J.M., Gallegos, C., 2006a. Thermorheological behaviour of a lithium lubricating grease. Tribol. Lett. 23, 47–54. https://doi.org/10.1007/s11249-006-9109-5.

Delgado, M.A., Valencia, C., Sánchez, M.C., Franco, J.M., Gallegos, C., 2006b. Influence of soap concentration and oil viscosity on the rheology and microstructure of lubricating greases. Ind. Eng. Chem. Res. 45, 1902–1910. https://doi.org/10.1021/ie050826f.

Delgado, M.A., Cortés-Triviño, E., Valencia, C., Franco, J.M., 2020. Tribological study of epoxide-functionalized alkali lignin-based gel-like biogreases. Tribol. Int. 146, 106231 https://doi.org/10.1016/j.triboint.2020.106231.

Ding, B., Li, C., Hotta, Y., Kim, J., Kuwaki, O., Shiratori, S., 2006. Conversion of an electrospun nanofibrous cellulose acetate mat from a super-hydrophilic to super-hydrophobic surface. Nanotechnology 17, 4332–4339. https://doi.org/10.1088/0957-4484/17/17/009.

Erdem, R., İlhan, M., Sancak, E., 2016. Analysis of EMSE and mechanical properties of sputter coated electrospun nanofibers. Appl. Surf. Sci. 380, 326–330. https://doi.org/10.1016/j.apsusc.2015.11.204.

Fajardo, C., Blánquez, A., Domínguez, G., Borrero-López, A., Valencia, C., Hernández, M., Arias, M., Rodríguez, J., 2021. Assessment of sustainability of bio treated lignocellulose-based oleogels. Polymers 13, 267. https://doi.org/10.3390/polym13020267.

Ferry, J.D., 1980. Viscoelastic properties of polymers, 3rd ed. New York.

Gallego, R., Arteaga, J.F., Valencia, C., Díaz, M.J., Franco, J.M., 2015a. Gel-Like dispersions of HMDI-cross-linked lignocellulosic materials in castor oil: toward completely renewable lubricating grease formulations. ACS Sustain. Chem. Eng. 3, 2130–2141. https://doi.org/10.1021/acssuschemeng.5b00389.

Gallego, R., Arteaga, J.F., Valencia, C., Franco, J.M., 2015b. Thickening properties of several NCO-functionalized cellulose derivatives in castor oil. Chem. Eng. Sci. 134, 260–268. https://doi.org/10.1016/j.ces.2015.05.007.

Gallego, R., Cidade, T., Sánchez, R., Valencia, C., Franco, J.M., 2016. Tribological behaviour of novel chemically modified biopolymer-thickened lubricating greases investigated in a steel–steel rotating ball-on-three plates tribology cell. Tribol. Int. 94, 652–660. https://doi.org/10.1016/j.triboint.2015.10.028.

Gellerstedt, G., Henriksson, G., 2008. Lignins: major sources, structure and properties. In: Monomers, Polymers and Composites from Renewable Resources. Elsevier, pp. 201–224. https://doi.org/10.1016/B978-0-08-045316-3.00009-0.

Heyer, P., Läuger, J., 2009. Correlation between friction and flow of lubricating greases in a new tribometer device. Lubr. Sci. 21, 253–268. https://doi.org/10.1002/ls.88.

Hotaling, N.A., Bharti, K., Kriel, H., Simon, C.G., 2015. DiameterJ: A validated open source nanofiber diameter measurement tool. Biomaterials 61, 327–338. https://doi.org/10.1016/j.biomaterials.2015.05.015.

Jedrzejczyk, M.A.Van, den Bosch, S., Van Aelst, J., Van Aelst, K., Kouris, P.D., Moalin, M., Haenen, G.R.M.M., Boot, M.D., Hensen, E.J.M., Lagrain, B., Sels, B.F., Bernaerts, K.V., 2021. Lignin-based additives for improved thermo-oxidative stability of biolubricants. ACS Sustain. Chem. Eng. 9, 12548–12559. https://doi.org/10.1021/acssuschemeng.1c02799.

Jia, H., Sun, N., Dirican, M., Li, Y., Chen, C., Zhu, P., Yan, C., Zang, J., Guo, J., Tao, J., Wang, J., Tang, F., Zhang, X., 2018. Electrospun kraft lignin/cellulose acetate-derived nanocarbon network as an anode for high-performance sodium-ion batteries. ACS Appl. Mater. Interfaces 10, 44368–44375. https://doi.org/10.1021/acsami.8b13033.

Kakoria, A., Sinha-Ray, S., 2018. A review on biopolymer-based fibers via electrospinning and solution blowing and their applications. Fibers 6, 45. https://doi.org/10.3390/fib6030045.

Kasprzycka-Guttman, T., Odzeniak, D., 1994. Antioxidant properties of lignin and its fractions. Thermochim. Acta 231, 161–168. https://doi.org/10.1016/0040-6031(94)80018-9.

Kaur, R., Uppal, S.K., 2015. Structural characterization and antioxidant activity of lignin from sugarcane bagasse. Colloid Polym. Sci. 293, 2585–2592. https://doi.org/10.1007/s00396-015-3653-1.

Kobayashi, H., Fukuoka, A., 2013. Synthesis and utilisation of sugar compounds derived from lignocellulosic biomass. Green. Chem. 15, 1740. https://doi.org/10.1039/c3gc00060e.

Konwarh, R., Karak, N., Misra, M., 2013. Electrospun cellulose acetate nanofibers: the present status and gamut of biotechnological applications. Biotechnol. Adv. 31, 421–437. https://doi.org/10.1016/j.biotechadv.2013.01.002.

Laurichesse, S., Avérous, L., 2014. Chemical modification of lignins: towards biobased polymers. Prog. Polym. Sci. 39, 1266–1290. https://doi.org/10.1016/j.progpolymsci.2013.11.004.

Lee, H., Nishino, M., Sohn, D., Lee, J.S., Kim, I.S., 2018. Control of the morphology of cellulose acetate nanofibers via electrospinning. Cellulose 25, 2829–2837. https://doi.org/10.1007/s10570-018-1744-0.

Liu, H., Hsieh, Y.-L., 2002. Ultrafine fibrous cellulose membranes from electrospinning of cellulose acetate. J. Polym. Sci. Part B Polym. Phys. 40, 2119–2129. https://doi.org/10.1002/polb.10261.

Madruga, L.Y.C., Kipper, M.J., 2021. Expanding the repertoire of electrospinning: new and emerging biopolymers, techniques, and applications. Adv. Healthc. Mater. 2101979. https://doi.org/10.1002/adhm.202101979.

Malm, J., Giannaras, D., Riehle, M.O., Gadegaard, N., Sjövall, P., 2009. Fixation and drying protocols for the preparation of cell samples for time-of-flight secondary ion mass spectrometry analysis. Anal. Chem. 81, 7197–7205. https://doi.org/10.1021/ac900636v.

Martín Alfonso, J.E., Yañez, R., Valencia, C., Franco, J.M., Díaz, M.J., 2009. Optimization of the methylation conditions of kraft cellulose pulp for its use as a thickener agent in biodegradable lubricating greases. Ind. Eng. Chem. Res. 48, 6765–6771. https://doi.org/10.1021/ie9002766.

Martín-Alfonso, J.E., Valencia, C., Sánchez, M.C., Franco, J.M., Gallegos, C., 2007. Development of new lubricating grease formulations using recycled LDPE as

rheology modifier additive. Eur. Polym. J. 43, 139–149. https://doi.org/10.1016/j.eurpolymj.2006.09.020.
Martín-Alfonso, J.E., Núñez, N., Valencia, C., Franco, J.M., Díaz, M.J., 2011. Formulation of new biodegradable lubricating greases using ethylated cellulose pulp as thickener agent. J. Ind. Eng. Chem. 17, 818–823. https://doi.org/10.1016/j.jiec.2011.09.003.
Mascal, M., Nikitin, E.B., 2010. Comment on processes for the direct conversion of cellulose or cellulosic biomass into levulinate esters. ChemSusChem 3, 1349–1351. https://doi.org/10.1002/cssc.201000326.
National Lubricating Grease Institute, 2006. NLGI Lubricating Greases Guide, 5th ed. Kansas City, MO, USA.
Nguyen, T.P.N., Yun, E.-T., Kim, I.-C., Kwon, Y.-N., 2013. Preparation of cellulose triacetate/cellulose acetate (CTA/CA)-based membranes for forward osmosis. J. Memb. Sci. 433, 49–59. https://doi.org/10.1016/j.memsci.2013.01.027.
Núñez, N., Martín-Alfonso, J.E., Eugenio, M.E., Valencia, C., Díaz, M.J., Franco, J.M., 2011. Preparation and characterization of gel-like dispersions based on cellulosic pulps and castor oil for lubricant applications. Ind. Eng. Chem. Res. 50, 5618–5627. https://doi.org/10.1021/ie1025584.
Núñez, N., Martín-Alfonso, J.E., Valencia, C., Sánchez, M.C., Franco, J.M., 2012. Rheology of new green lubricating grease formulations containing cellulose pulp and its methylated derivative as thickener agents. Ind. Crops Prod. 37, 500–507. https://doi.org/10.1016/j.indcrop.2011.07.027.
Oliveira, M.S.N., Yeh, R., McKinley, G.H., 2006. Iterated stretching, extensional rheology and formation of beads-on-a-string structures in polymer solutions. J. Nonnewton. Fluid Mech. 137, 137–148. https://doi.org/10.1016/j.jnnfm.2006.01.014.
Panchal, T.M., Patel, A., Chauhan, D.D., Thomas, M., Patel, J.V., 2017. A methodological review on bio-lubricants from vegetable oil based resources. Renew. Sustain. Energy Rev. 70, 65–70. https://doi.org/10.1016/j.rser.2016.11.105.
Pelaez-Samaniego, M.R., Yadama, V., Garcia-Perez, M., Lowell, E., Zhu, R., Englund, K., 2016. Interrelationship between lignin-rich dichloromethane extracts of hot water-treated wood fibers and high-density polyethylene (HDPE) in wood plastic composite (WPC) production. Holzforschung 70, 31–38. https://doi.org/10.1515/hf-2014-0309.
Polman, E.M.N., Gruter, G.J.M., Parsons, J.R., Tietema, A., 2020. Comparison of the aerobic biodegradation of biopolymers and the corresponding bioplastics: a review. Sci. Total Environ. 753, 141953 https://doi.org/10.1016/j.scitotenv.2020.141953.
Prasad, A., Sotenko, M., Blenkinsopp, T., Coles, S.R., 2016. Life cycle assessment of lignocellulosic biomass pretreatment methods in biofuel production. Int. J. Life Cycle Assess. 21, 44–50. https://doi.org/10.1007/s11367-015-0985-5.
Quinchia, L.A., Delgado, M.A., Valencia, C., Franco, J.M., Gallegos, C., 2010. Viscosity modification of different vegetable oils with EVA copolymer for lubricant applications. Ind. Crops Prod. 32, 607–612. https://doi.org/10.1016/j.indcrop.2010.07.011.
Rubio-Valle, J.F., Sánchez, M.C., Valencia, C., Martín-Alfonso, J.E., Franco, J.M., 2021. Electrohydrodynamic processing of pvp-doped kraft lignin micro- and nano-structures and application of electrospun nanofiber templates to produce oleogels. Polymers (Basel) 13, 2206. https://doi.org/10.3390/polym13132206.
Rubio-Valle, J.F., Jiménez-Rosado, M., Perez-Puyana, V., Guerrero, A., Romero, A., 2021. Electrospun nanofibres with antimicrobial activities. In: Antimicrobial Textiles from Natural Resources. Elsevier, pp. 589–618. https://doi.org/10.1016/B978-0-12-821485-5.00020-2.
Sánchez, R., Stringari, G.B., Franco, J.M., Valencia, C., Gallegos, C., 2011. Use of chitin, chitosan and acylated derivatives as thickener agents of vegetable oils for bio-lubricant applications. Carbohydr. Polym. 85, 705–714. https://doi.org/10.1016/j.carbpol.2011.03.049.
Sánchez, R., Valencia, C., Franco, J.M., 2014. Rheological and tribological characterization of a new acylated chitosan–based biodegradable lubricating grease: a comparative study with traditional lithium and calcium greases. Tribol. Trans. 57, 445–454. https://doi.org/10.1080/10402004.2014.880541.
Stojanovska, E., Pampal, E.S., Kilic, A., Quddus, M., Candan, Z., 2019. Developing and characterization of lignin-based fibrous nanocarbon electrodes for energy storage devices. Compos. Part B Eng. 158, 239–248. https://doi.org/10.1016/j.compositesb.2018.09.072.
Stokroos, I., Kalicharan, D., Van Der Want, J.J., Jongebloed, W.L., 1998. A comparative study of thin coatings of Au/Pd, Pt and Cr produced by magnetron sputtering for FE-SEM. J. Microsc. 189, 79–89. https://doi.org/10.1046/j.1365-2818.1998.00282.x.
Syahir, A.Z., Zulkifli, N.W.M., Masjuki, H.H., Kalam, M.A., Alabdulkarem, A., Gulzar, M., Khuong, L.S., Harith, M.H., 2017. A review on bio-based lubricants and their applications. J. Clean. Prod. 168, 997–1016. https://doi.org/10.1016/j.jclepro.2017.09.106.
Tuomela, M., Vikman, M., Hatakka, A., Itävaara, M., 2000. Biodegradation of lignin in compost: a review. Bioresour. Technol. 72, 169–183. https://doi.org/10.1016/S0960-8524(99)00104-2.
Vangeel, T., Schutyser, W., Renders, T., Sels, B.F., 2018. Perspective on lignin oxidation: advances, challenges, and future directions. Top. Curr. Chem. 376, 30. https://doi.org/10.1007/s41061-018-0207-2.
Wilk, S., Benko, A., 2021. Advances in fabricating the electrospun biopolymer-based biomaterials. J. Funct. Biomater. 12, 26. https://doi.org/10.3390/jfb12020026.
Xi, Y., Yang, D., Qiu, X., Wang, H., Huang, J., Li, Q., 2018. Renewable lignin-based carbon with a remarkable electrochemical performance from potassium compound activation. Ind. Crops Prod. 124, 747–754. https://doi.org/10.1016/j.indcrop.2018.08.018.
Zeng, J., Haoqing, H., Schaper, A., Wendorff, J.H., Greiner, A., 2003. Poly-L-lactide nanofibers by electrospinning – influence of solution viscosity and electrical conductivity on fiber diameter and fiber morphology. e-Polymers 3. https://doi.org/10.1515/epoly.2003.3.1.102.
Zhang, X., Wang, B., Qin, X., Ye, S., Shi, Y., Feng, Y., Han, W., Liu, C., Shen, C., 2020. Cellulose acetate monolith with hierarchical micro/nano-porous structure showing superior hydrophobicity for oil/water separation. Carbohydr. Polym. 241, 116361 https://doi.org/10.1016/j.carbpol.2020.116361.